Supplementary information

Supplementary information

Engineering a Semi-Artificial Photosynthetic Biofilm for Robust and High-Efficiency CO_2-to-Methane Conversion

Huize Chen[a, b], Ao Xia*[a, b], Yun Huang[a, b], Junyi Ji[c], Jingmiao Zhang[a, b], Xianqing Zhu[a, b], Xun Zhu[a, b], Qiang Liao[a, b]

[a] Key Laboratory of Low-grade Energy Utilization Technologies and Systems, Chongqing University, Chongqing 400044, China

[b] School of Energy and Power Engineering, Chongqing University, Chongqing 400044, China

[c] School of Chemical Engineering, Sichuan University, Chengdu 610065, China

Supplementary information

Section SI. Experimental Section

Synthesis of Hybrid Biofilms

Graphitic carbon nitride (CN_x) was synthesized via thermal calcination of melamine. The precursor was placed in a tube furnace (OTF-1200X-S, Hefei Kejing, Hefei, China) and heated under an air atmosphere. The temperature was ramped to 520 °C at a rate of 2°C/h and held for 2 h, followed by a subsequent hold at 550 °C for an additional 2 h. The process yielded the final product with a mass yield of approximately 30% [1]. The obtained CN_x was ground and mixed with potassium thiocyanate (KSCN) at a 1:2 mass ratio. The mixture underwent secondary calcination under Ar atmosphere with a heating rate of 20 °C/h, followed by heating at 400 °C and 500 °C for 1 h and 0.5 h [2]. The $^{NCN}CN_x$ was ultrasonically dispersed in deionized water (200 W, 10s work, 10s off, for 30 cycles), followed by four centrifugal washing cycles (10000 rpm, 10 min each), and freeze-dried for 24 h (Figure S1).

Methanosarcina barkeri (CCAM 8200, China Center for Preservation and Management of Anaerobic Microorganism Resources) was cultured in modified 120 mediums (Table S1) (35°C, pH=6.8) [3]. When *M. barkeri* reached the exponential phase (OD600≈0.4), 50 mL of the suspension was centrifuged three times using anaerobic saline, then resuspended in 20 mL of saline, and 0.06 g of $^{NCN}CN_x$ was added to obtain the hybrid [4]. 1 mL of hybrid and 1 mL of illuminated culture medium (Table S2) were added to a 20 mL anaerobic vial. After one day of dark cultivation, the vials were placed in a constant temperature chamber (35 °C) equipped with 395±5 nm LED light sources to initiate the light exposure experiment. The experimental group with added Ag-NPs received 0.5 mL of Ag-NPs particle solution (20 nm, >0.75 A520 Units/ml) in 50 mL of *M. barkeri* culture during the early stage, while the control group was supplemented with anoxic water to equalize the volume. All anaerobic operations were performed in an anaerobic glove box (Concept-400, Barker, USA). The *M. barkeri* suspension was centrifuged at 7500 rpm for 10 minutes. The supernatant was discarded, and PBS solution was added, followed by heating in a water bath for 1 h. The mixture was centrifuged at 9000 rpm for 20 minutes, and the supernatant was collected as the EPS extract [5].

Methanogenesis experiments

The methanogenesis experiments under light were conducted in 20 mL anaerobic vials (2 mL liquid phase volume, 18 mL headspace volume). A set of three parallel samples, wrapped with black light-shielding tape on the sides, were placed 15 cm above a surface light source composed of 395±5 nm LED lamps, ensuring only the bottom of the vials received uniform radiation intensity. The voltage of the LED beads was adjusted, and used a UV irradiance meter calibrated at 395 nm (LS125, linshangtech, China) to control the UV power density received at the bottom of the bottle. When investigating the protective effect of extracellular polymer substances on cells under UV irradiation (2.7 mW/cm^2), the experimental group was supplemented with 0.5 mL of EPS extract, while the control group was adjusted to volume using oxygen-free deionized water.

Characterization

The functional group information of the hybrid system was analyzed using an FT-IR spectrometer (Nicolet 6700, Thermo Fisher Scientific, USA) (wavenumber range: 400–4000 cm^{-1}, spectral resolution: 4 cm^{-1}, signal-to-noise ratio: 50,000:1, scans: 32. The hybrid system's liquid-phase organic components were analyzed using a steady-state/transient fluorescence spectrometer (FLS1000, Edinburgh Instruments, UK) (Excitation wavelength scan range: 220–450, Emission wavelength scan range: 220–600 nm, excitation wavelength interval: 5 nm, emission wavelength interval: 2 nm, scan speed: 1200 nm/min, excitation/emission slit width: 5 nm). X-ray diffraction (XRD) data were collected (D8 ADVANCE, Bruker, Germany) at 40 kV and 40 mA. High-resolution transmission electron microscopy (HR-TEM) images were acquired (Tecnai G2 F30 instrument, FEI, USA). Scanning electron microscope (SEM) images of the hybrid system were obtained (Tescan, Czech Republic). Elemental mapping was performed using an energy-dispersive X-ray spectroscopy (EDS) system attached to the TEM. Confocal laser scanning microscopy (CLSM) images were acquired using a confocal laser scanning microscope (TCS SP8, Leica, Germany). The material's absorption spectrum was measured using a UV-Vis-NIR spectrophotometer (UV-3600, SHIMADZU, Japan). X-ray Photoelectron Spectroscopy (XPS) analyses were performed (250Xi, Thermo escalab, USA), equipped with a monochromatic Al Kα X-ray source (hv = 1486.6 eV). The source was operated at a power of 150 W with a 650 μm spot size. The applied voltage and current were 14.8 kV and 1.6 A, respectively. For charge correction, all binding energies were referenced to the adventitious carbon C 1s peak at 284.8 eV.

Supplementary information

The binding interactions of *M. barkeri* with $^{NCN}CN_x$ and with extracellular polymeric substances were characterized using a high-sensitivity Nano Isothermal Titration Calorimeter (Nano-ITC, TA, USA). For these titrations, 8 μL aliquots of an *M. barkeri* suspension were injected into either the $^{NCN}CN_x$ solution or the EPS solution at 300 s intervals [6]. The sample acidified $^{NCN}CN_x$ ($^{NCN}CN_x$-HCl) was obtained by stirring 50 mg $^{NCN}CN_x$ in 20 mL 1 M HCl aqueous solution for three hours, followed by repeated washing with deionized water and subsequent freeze-drying. Electrochemical characterizations were conducted in a three-electrode anaerobic electrochemical quartz cell connected to a CHI 660E electrochemical workstation (CH Instruments, Austin, TX, USA). The hybrid material was drop-cast onto carbon paper, dried at 35 °C, and then used as the working electrode. A 1 cm×1 cm platinum sheet and a saturated calomel electrode (SCE) housed within a salt bridge were used as the counter and reference electrodes, respectively. Cyclic voltammetry (CV) curves were recorded within the potential range of −1.0 V to +0.5 V (vs. SCE) at a scan rate of 10 mV/s.

Proteomic analysis was performed on cell pellets collected from samples *M. barkeri*-$^{NCN}CN_x$ and Ag@ *M. barkeri*-$^{NCN}CN_x$ after 72h illumination experiment [7]. Following digestion, peptides were labeled using iTRAQ reagents (AB Sciex). These labeled peptides were then analyzed using an EASY-nLC 1200 system coupled to a Q-Exactive mass spectrometer (Thermo Fisher Scientific). Thermo Xcalibur software was used for raw data collection, and Sequest HT (Thermo Fisher Scientific) was employed for subsequent data analysis. The complete proteomic dataset has been deposited to the ProteomeXchange Consortium via the iProx partner repository under the identifier PXD013207. Additionally, transmembrane helices were predicted with TMHMM, protein subcellular localization with PSORTb, and the presence of signal peptides with SignalP.

Measurements

The impact of nanosilver particle addition on cell viability was assessed using live/dead cell staining (EX300, Solarbio, China). The oxidative stress status of cells with/without EPS was assessed using DCFH-DA (Solarbio, China). Fluorescence images were analyzed using ImageJ software. The concentration of gas components in the headspace of the anaerobic bottle is determined using a gas chromatograph (TRACE 1300, Thermo Fisher Scientific, USA). The MDA and H_2O_2 of the hybrid biofilm system under different intensities of UV light were determined using assay kits (MDA assay kits, Solarbio, China; H_2O_2 assay kits, Nanjing Jiancheng, China). The average quantum yield (QY) was determined using a previously reported method as shown in Eq. (S1) [8].

$$\mathrm{QY} = \frac{Number\ of\ electrons\ required\ for\ CO_2\ methanation}{Number\ of\ photons\ injected\ into\ the\ hybrid\ system} \times 100\% = \frac{8 \times n(CH_4)}{\frac{P_{light} \times A_{\mathrm{vial}} \times T \times \lambda}{h \times c}} \times 100\% \quad \text{(S1)}$$

where $n(CH_4)$ is the number of methane molecules produced, P_{light} is the incident light's power density, A_{vial} is the illuminated area at the bottom of the anaerobic vial (4.987 cm^2), T is the illumination time, λ is the light wavelength (395 nm), h is the Planck constant, c is the speed of light.

The methane selectivity was determined using a previously reported method, following the equation below [8].

$$\mathrm{Selectivity} = \frac{Number\ of\ electrons\ required\ for\ CO_2\ methanation}{Number\ of\ electrons\ required\ for\ methane\ and\ hydrogen\ production} \times 100\% \quad (2)$$

Modeling

The transport of radiation within the medium under investigation is modeled by the steady-state Radiative Transfer Equation (RTE), following the equation below.

$$S_i \cdot \nabla l_i(r) = -\beta(i) l_i(r) + \frac{\sigma_s(r)}{4\pi} \sum_{j=1}^{N} \omega_j l_j(r) \phi(S_i, S_i) \quad (3)$$

where r is the spatial position vector. $l_i(r)$ is the radiance at position r in the i-th discrete direction S_i. S_i is the unit vector representing the i-th discrete angular direction. $\beta(i)$ is the extinction coefficient, defined as the sum of the absorption coefficient $\sigma_a(r)$and the scattering coefficient $\sigma_s(r)$. $\sigma_s(r)$ is the scattering coefficient. ω_j are the quadrature weights associated with the j-th discrete direction. $\phi(S_i, S_i)$ is the scattering phase function, which describes the probability that radiation incident from direction S_j is scattered into direction S_i (for this study, an isotropic phase function, $\phi(S_i, S_j)$=1, was assumed). N is the total number of discrete directions used in the angular discretization.

Supplementary information

The incident radiation, $G(r)$, also known as the fluence rate, at a point r is calculated by integrating the radiance over all 4π steradians, which in its discretized form is:

$$G(r) = \sum_{i=1}^{N} \omega_i l_i(r) \quad (4)$$

The numerical simulations were performed within a two-dimensional (2D) rectangular computational domain. This domain was designed to represent a cross-section of the experimental setup. The base of the domain, with a length of 25.2 mm, was defined as the incident surface for incoming radiation. Above this incident surface, two distinct layers were modeled: a biofilm layer with a uniform thickness of 0.2 mm (200 μm) was situated directly adjacent to the incident surface. A suspension bulk with a height of 4.0 mm. All other boundaries of the rectangular domain (i.e., the top surface and the two vertical sides) were treated as perfectly absorbing blackbody surfaces. This condition ensures that any radiation reaching these boundaries is fully absorbed, and no reflection or transmission occurs. The parameter settings used for the modeling are provided in Table S3.

Section SII. Supporting Figures and Tables

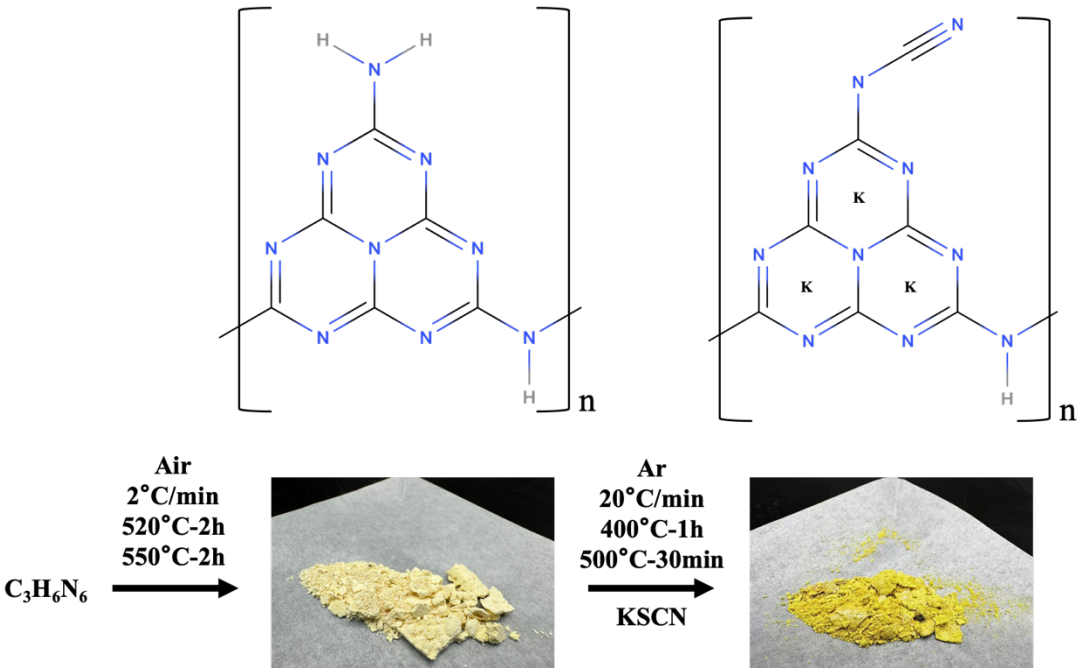

Figure S1. Preparation procedures, material images, and molecular formulas for CN_x and $^{NCN}CN_x$.

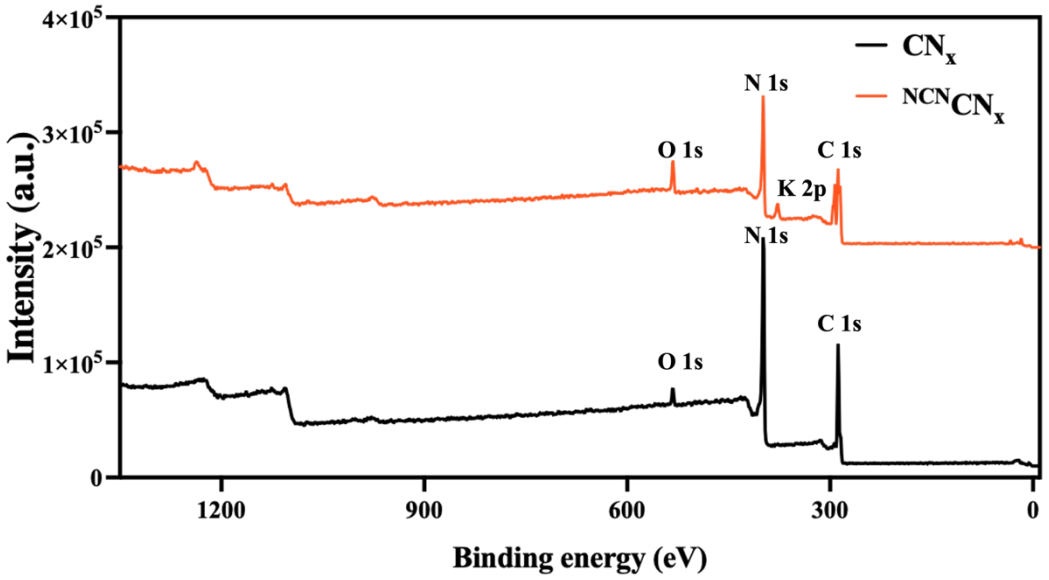

Figure S2. X-ray Photoelectron Spectroscopy (XPS) survey spectra of CN_x and $^{NCN}CN_x$.

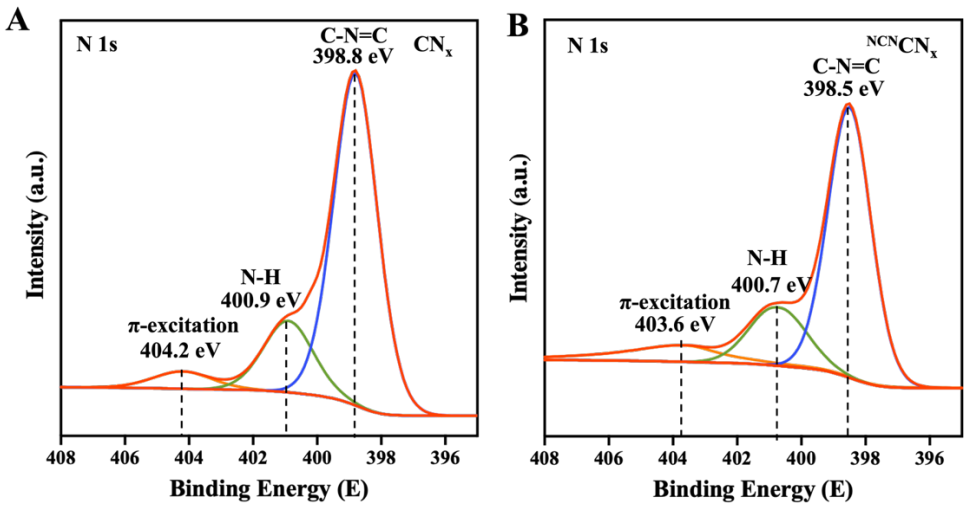

Figure S3. The N1s XPS spectra of A) CN_x, B) $^{NCN}CN_x$.

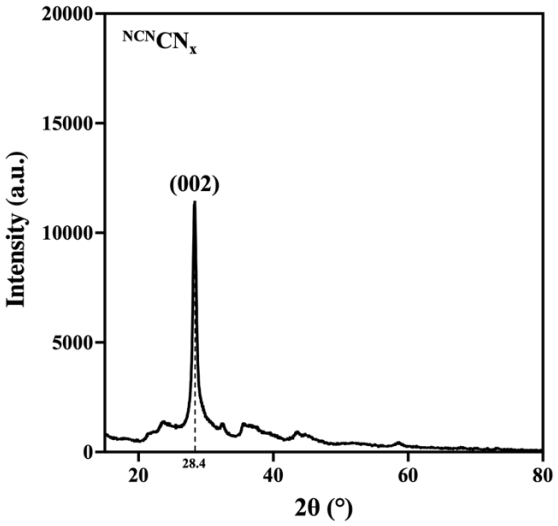

Figure S4. X-ray diffraction (XRD) pattern of $^{NCN}CN_x$.

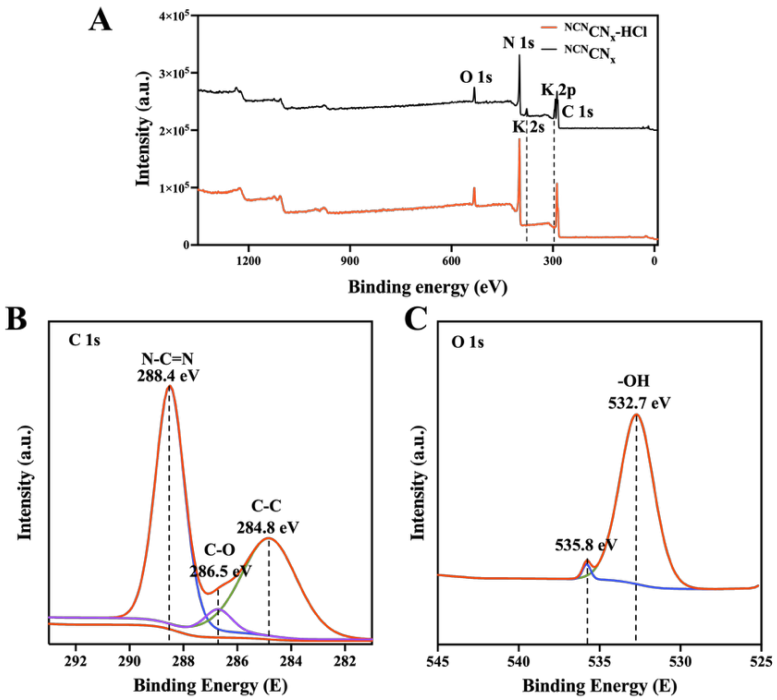

Figure S5. A) Disappearance of the XPS signal for potassium after acid treatment. B) The C1s XPS spectra of acid-treated $^{NCN}CN_x$, the cyano group is eliminated. C) The O1s XPS spectra of acid-treated $^{NCN}CN_x$, the peak centered at 535.8 eV is attributed to adsorbed water [9].

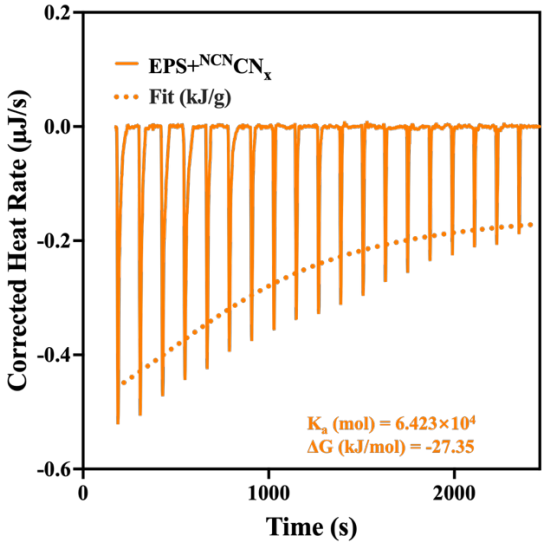

Figure S6. ITC thermogram of the interactions between EPS and $^{NCN}CN_x$, the dashed line represents the fitting result.

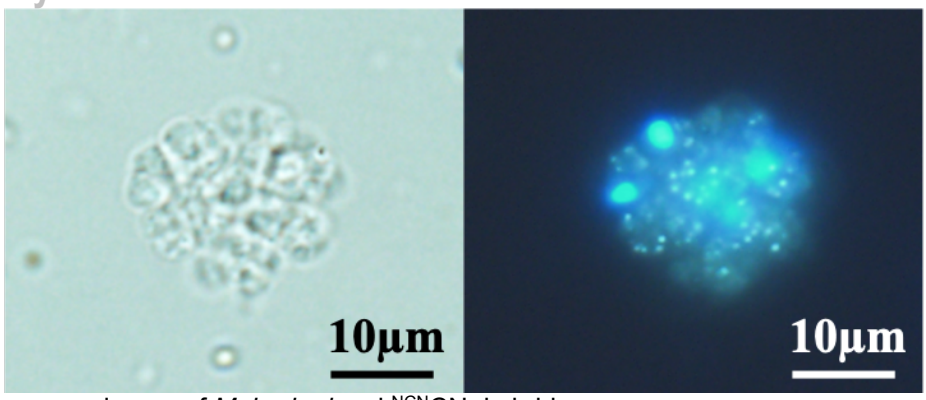

Figure S7. Fluorescence image of *M. barkeri* and $^{NCN}CN_x$ hybrids.

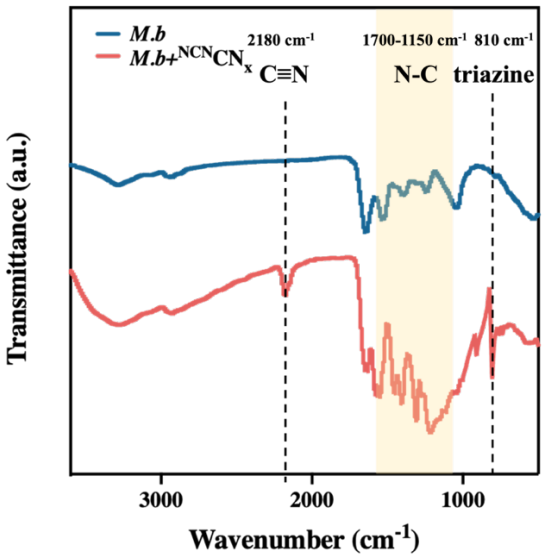

Figure S8. FTIR spectra of *M. barkeri* and *M. barkeri*+$^{NCN}CN_x$.

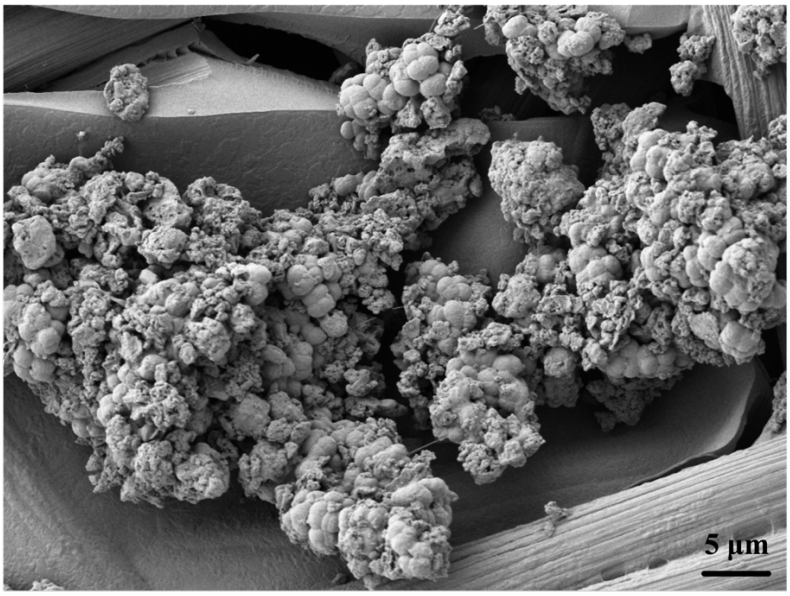

Figure S9. SEM image of the aggregate hybrid biofilm formed by *M. barkeri* cells and $^{NCN}CN_x$.

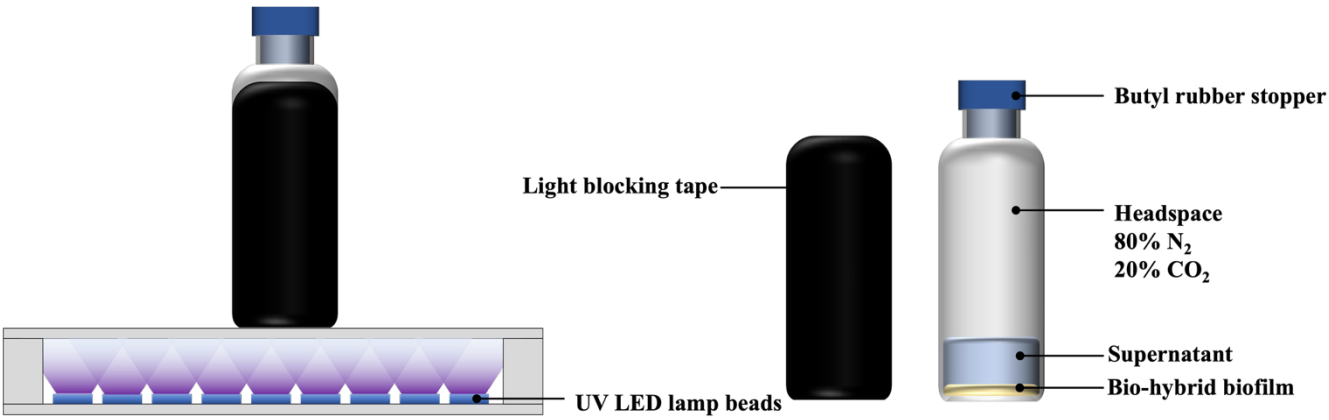

Figure S10. Lighting experiment setup.

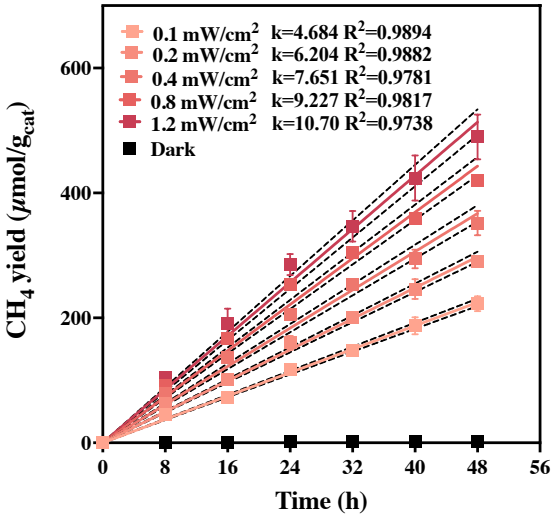

Figure S11. Linear fitting results for methane production under different light intensities, along with the fitted slope k and R^2 (the dashed lines show the 95% confidence bands.).

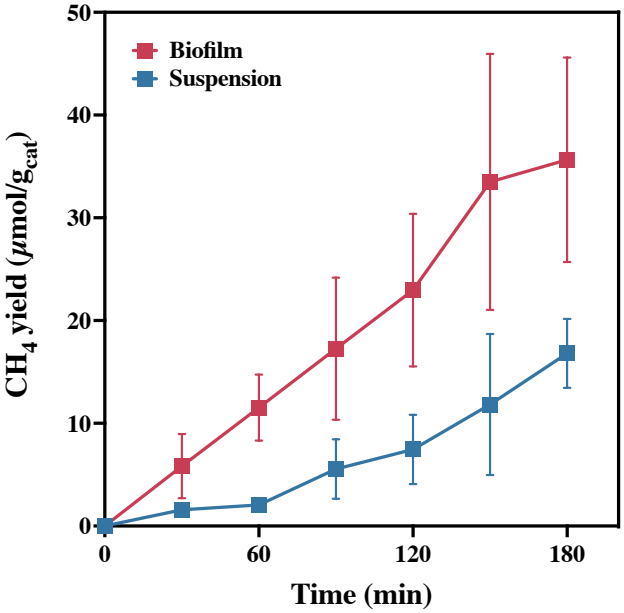

Figure S12. Comparison of methane production between the suspension and biofilm states.

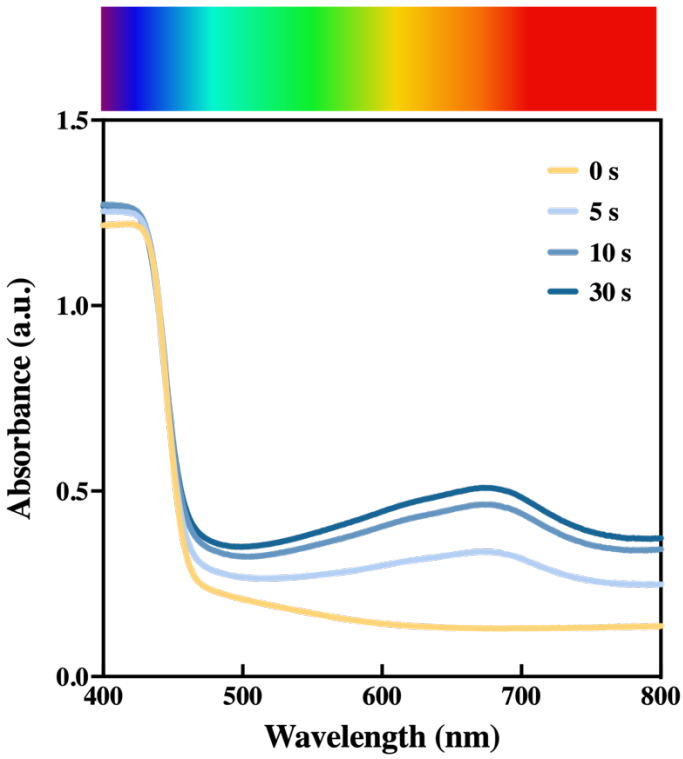

Figure S13. Visible light absorption characteristics of $^{NCN}CN_x$ after UV irradiation for different durations.

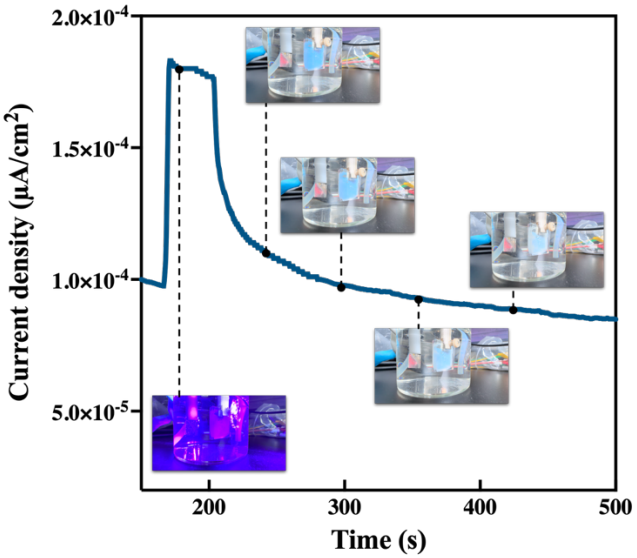

Figure S14. Synchronicity between the decolorization process of the blue biofilm and the electron release process.

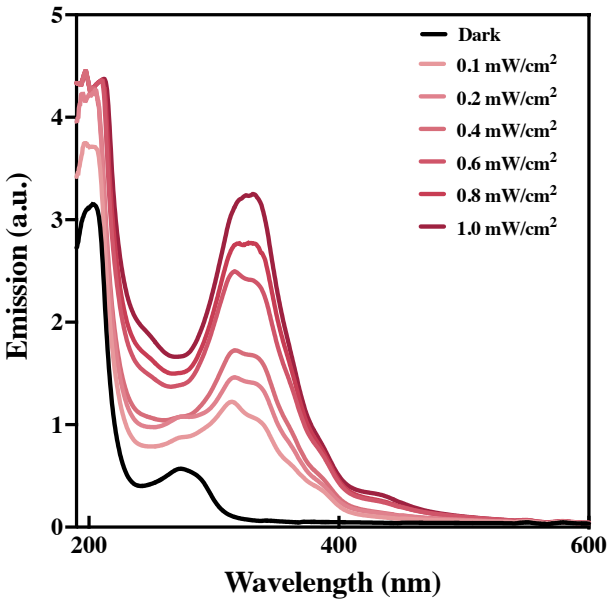

Figure S15. UV-Vis absorption spectra of the bulk liquid under different light intensities.

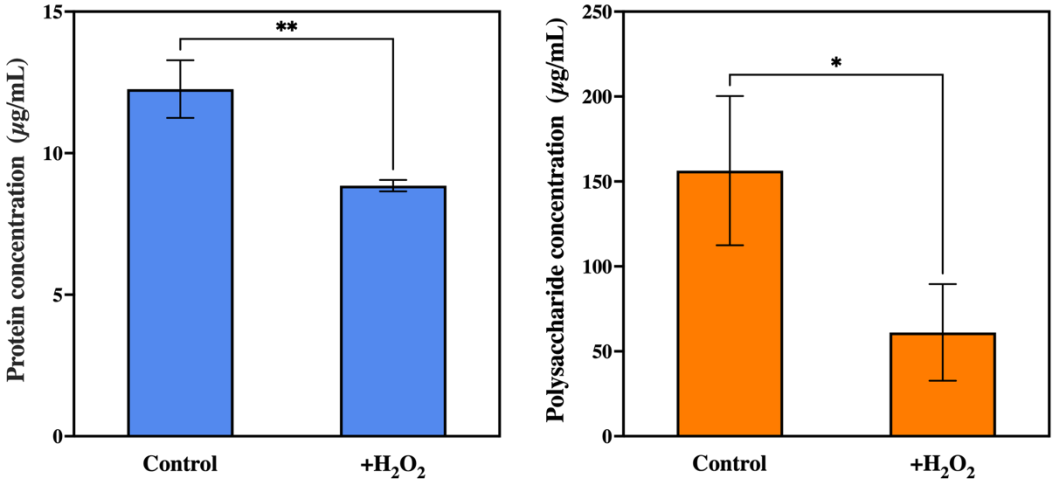

Figure S16. Changes in the concentrations of polysaccharide and protein components of EPS after 6 hours of incubation with hydrogen peroxide.

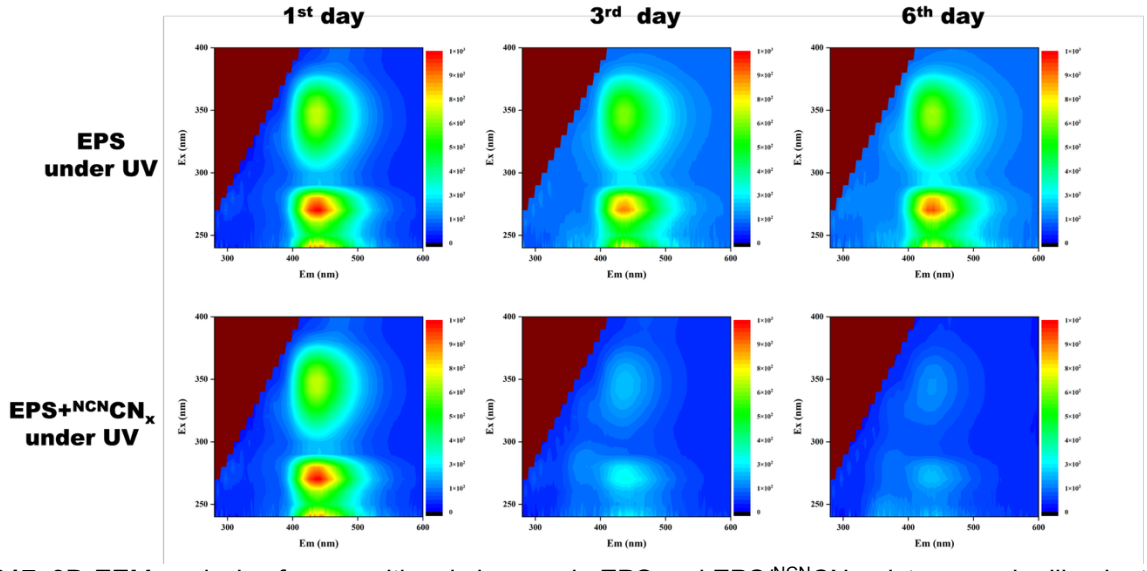

Figure S17. 3D-EEM analysis of compositional changes in EPS and EPS/$^{NCN}CN_x$ mixtures under illumination.

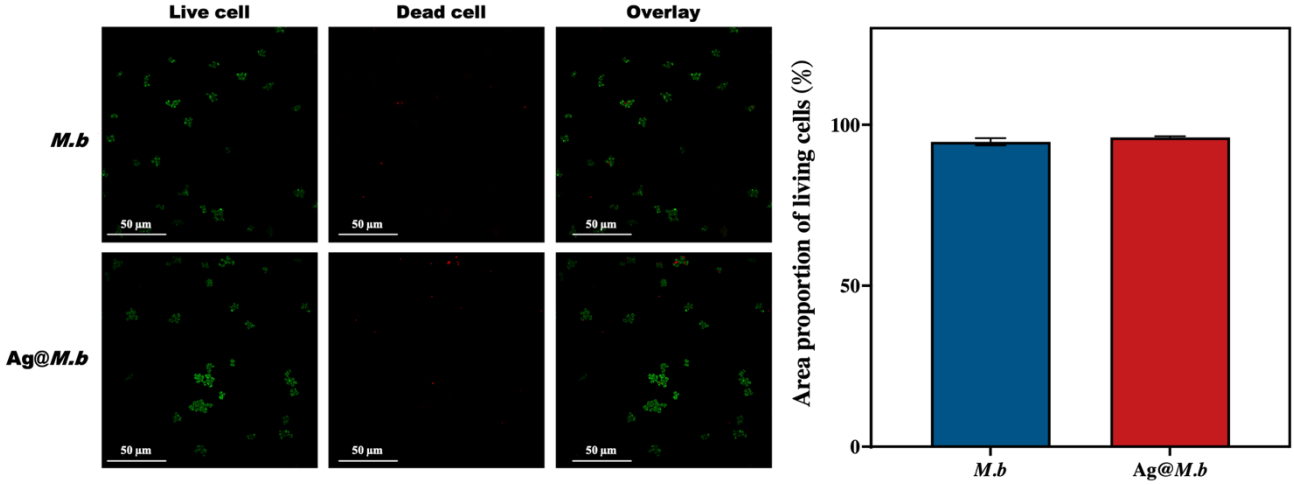

Figure S18. Effect of the addition of nanosilver on the ratio of stained live/dead cells.

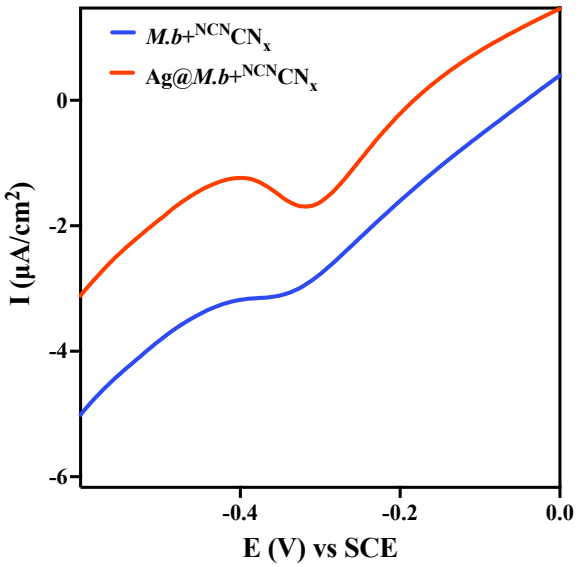

Figure S19. Voltammograms of hybrid biofilms with and without nanosilver addition.

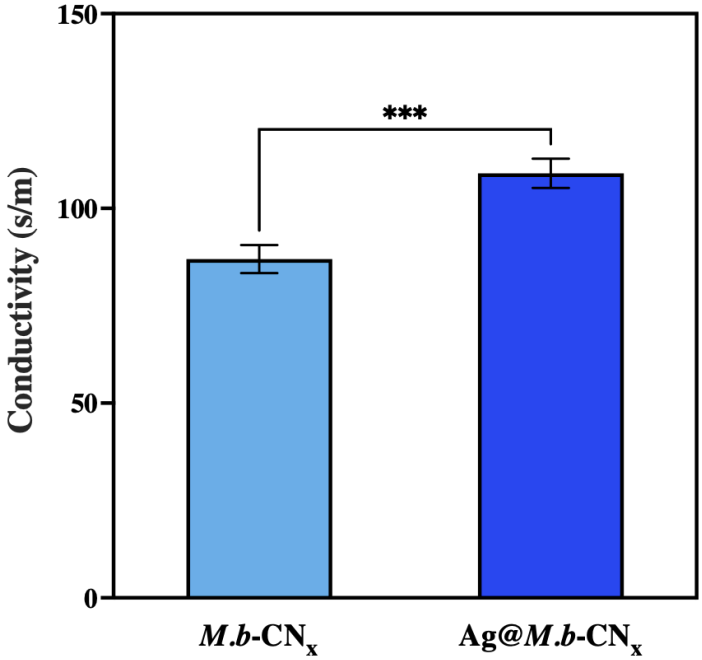

Figure S20. Effect of nanosilver addition on the electrical conductivity of hybrid biofilms.

Supplementary information

Table S1 Modified 120 medium [3]

Ingredients	Content
K_2HPO_4	0.35 g
KH_2PO_4	0.23 g
NH_4Cl	0.5 g
$MgSO_4 \cdot 7H_2O$	0.5 g
$CaCl_2 \cdot 2H_2O$	0.25 g
NaCl	2.25 g
$FeSO_4 \cdot 7H_2O$ solution (0.1% w/v)*	2 mL
Trace Element Solution SL-10**	1 mL
Yeast extract powder	2 g
Casein peptone	2 g
Na-acetate	2.5 g
$NaHCO_3$	2 g
Methanol	10 mL
Wolin's vitamin solution (10x)***	1 mL
L-Cysteine HCl $\cdot H_2O$	0.3 g
$Na_2S \cdot 9H_2O$	0.3 g
Oxygen-free deionized water	1000 mL

(Wolin's vitamin solution, L-Cysteine HCl $\cdot H_2O$, $Na_2S \cdot 9H_2O$, Methanol, $NaHCO_3$ were added through a filter (0.22 μm) after steam sterilization.)

*Each liter of $FeSO_4 \cdot 7H_2O$ solution (0.1% w/v) contains 1 g of $FeSO_4 \cdot 7H_2O$ and 1000 mL of 0.05 mol/L H_2SO_4.

**Each liter of SL-10 trace element solution contains: 10 ml of 25% HCl, 1.35 g $FeCl_2 \cdot 4H_2O$, 63 mg $ZnCl_2$, 90 mg $MnCl_2 \cdot 4H_2O$, 5.4 mg H_3BO_3, 171 mg $CoCl_2 \cdot 6H_2O$, 1.8 mg $CuCl_2 \cdot 2H_2O$, 21.6 mg $NiCl_2 \cdot 6H_2O$, 32.4 mg $Na_2MoO_4 \cdot 2H_2O$.

***Each liter of Wolin vitamin solution (10X concentrate) contains 20.0 mg biotin, 20.0 mg folic acid, 100.0 mg pyridoxine hydrochloride, 50.0 mg thiamine HCl, 50.0 mg riboflavin, 50.0 mg nicotinic acid, 50.0 mg Calcium D-(+)-pantothenate, 1.0 mg vitamin B_{12}, 50.0 mg p-Aminobenzoic acid, and 50.0 mg (DL)-alpha-lipoic acid.

Table S2 Illuminated culture medium

Ingredients	Content
$MgCl_2 \cdot 6H_2O$	0.8 g
$CaCl_2 \cdot 2H_2O$	0.2 g
NH_4Cl	0.2 g
KH_2PO_4	0.4 g
KCl	1.0 g
HEPES	14.32 g
$NaHCO_3$	5 g
Cysteine-HCl	0.48 g
Trace element solution SL-10	2 mL
Selenite-tungstate solution*	2 mL
Wolin's vitamin solution (10x)	0.6 mL

* Each liter of selenite-tungstate solution: 0.5g NaOH, 3.0mg $Na_2SeO_3 \cdot 5H_2O$, 4.0mg $Na_2WO_4 \cdot 2H_2O$.

Table S3 Modeling parameter settings

Symbol	Value	Unit	Description
D_{bottom}	0.0252	m	Bottle bottom diameter
H_{bulk}	0.0040	m	Liquid height
I_0	10	$W \cdot cm^{-2}$	Initial intensity
σ_a-water	0.0090	m^{-1}	Absorption coefficient of water
σ_a-sus	612	m^{-1}	Absorption coefficient of hybrid suspension
σ_a-bio	3769	m^{-1}	Absorption coefficient of hybrid biofilm
σ_s-water	0.0120	m^{-1}	Scattering coefficient of water
σ_s-sus	3.11	m^{-1}	Scattering coefficient of hybrid suspension
σ_s-bio	3815	m^{-1}	Scattering coefficient of hybrid biofilm

Table S4 Comparison of photosynthetic performance of *M. barkeri*-based biohybrid systems.

Photosensitizer	Light Source	Light Intensity (mW/cm^2)	CH_4 Production Rate ($\mu mol/g_{cat}/d$)	AQY (%)	Selectivity (%)	Stability (d)	Ref.
Carbon nitride	395 nm	0.8	48.6	0.67	92.3	20	[4]
M.b/CdS	395 nm	1.07	37.4	0.34	N.R.	5	[10]
Carbon nitride/BBR	365 nm	5.0	217.8	0.4	N.R.	6	[11]
CdS/Ni	395 nm	0.8	807.5	0.75	N.R.	6	[7]
Carbon nitride/BP	395 nm	0.8	77.0	1.26	N.R.	10	[12]
G.s/ Carbon nitride	AM 1.5	100	22.1	N.R.	N.R.	5	[13]
Ag/Carbon nitride	395 nm	0.1	141.9	1.92	97.1	14	This study

Note: All performance metrics were calculated based on continuous illumination.
N.R.: Not reported in the cited reference.

References

1. J. Fang, D. Wang, H. Xu, F. Sun, Y. Fan, R. Chen and Q. Liu, Unleashing solar energy's full potential: Synergetic thermo-photo catalysis for enhanced hydrogen production with metal-free carbon nitrides, *Energy Conversion and Management*, 2024, **300**, 117995. https://doi.org/10.1016/j.enconman.2023.117995
2. H. Kasap, D. S. Achilleos, A. Huang and E. Reisner, Photoreforming of Lignocellulose into H_2 Using Nanoengineered Carbon Nitride under Benign Conditions, *Journal of the American Chemical Society*, 2018, **140**, 11604-11607. https://doi.org/10.1021/jacs.8b07853
3. R. Xia, J. Cheng, Z. Chen, Z. Zhang, X. Zhou, J. Zhou and M. Zhang, Revealing Co-N4@Co-NP Bridge-Enabled Fast Charge Transfer and Active Intracellular Methanogenesis in Bio-Electrochemical CO2-Conversion with Methanosarcina Barkeri, *Advanced Materials*, 2023, **35**, 2304920. https://doi.org/10.1002/adma.202304920
4. A. Hu, J. Ye, G. Ren, Y. Qi, Y. Chen and S. Zhou, Metal-Free Semiconductor-Based Bio-Nano Hybrids for Sustainable CO_2-to-CH_4 Conversion with High Quantum Yield, *Angewandte Chemie International Edition*, 2022, **61**, e202206508. https://doi.org/10.1002/anie.202206508
5. C. Gu, P. Gao, F. Yang, D. An, M. Munir, H. Jia, G. Xue and C. Ma, Characterization of extracellular polymeric substances in biofilms under long-term exposure to ciprofloxacin antibiotic using fluorescence excitation-emission matrix and parallel factor analysis, *Environmental Science and Pollution Research*, 2017, **24**, 13536-13545. https://doi.org/10.1007/s11356-017-8986-5
6. F. Loosli, L. Vitorazi, J.-F. Berret and S. Stoll, Towards a better understanding on agglomeration mechanisms and thermodynamic properties of TiO_2 nanoparticles interacting with natural organic matter, *Water Research*, 2015, **80**, 139-148. https://doi.org/10.1016/j.watres.2015.05.009
7. J. Ye, G. Ren, L. Kang, Y. Zhang, X. Liu, S. Zhou and Z. He, Efficient Photoelectron Capture by Ni Decoration in *Methanosarcina barkeri*-CdS Biohybrids for Enhanced Photocatalytic CO_2-to-CH_4 Conversion, *iScience*, 2020, **23**. https://doi.org/10.1016/j.isci.2020.101287
8. M. Chen, Q. Cai, X. Chen, S. Huang, Q. Feng, T. Majima, R. J. Zeng and S. Zhou, Anthraquinone-2-Sulfonate as a Microbial Photosensitizer and Capacitor Drives Solar-to-N_2O Production with a Quantum Efficiency of Almost Unity, *Environmental Science & Technology*, 2022, **56**, 5161-5169. https://doi.org/10.1021/acs.est.1c08710
9. S. D. Gardner, C. S. K. Singamsetty, G. L. Booth, G.-R. He and C. U. Pittman, Surface characterization of carbon fibers using angle-resolved XPS and ISS, *Carbon*, 1995, **33**, 587-595. https://doi.org/10.1016/0008-6223(94)00144-O
10. J. Ye, J. Yu, Y. Zhang, M. Chen, X. Liu, S. Zhou and Z. He, Light-driven carbon dioxide reduction to methane by Methanosarcina barkeri-CdS biohybrid, *Applied Catalysis B: Environmental*, 2019, **257**, 117916. https://doi.org/10.1016/j.apcatb.2019.117916
11. W. Gu, J. Hu, L. Li, M. Hong, C. Yang, G. Ren, J. Ye and S. Zhou, Natural AIEgens as Ultraviolet Sunscreens and Photosynergists for Solar Fuel Production, *Environmental Science & Technology*, 2024, **58**, 20434-20443. https://10.1021/acs.est.4c05605
12. A. Hu, T. Fu, G. Ren, M. Zhuang, W. Yuan, S. Zhong and S. Zhou, Sustained Biotic-Abiotic Hybrids Methanogenesis Enabled Using Metal-Free Black Phosphorus/Carbon Nitride, *Frontiers in Microbiology*, 2022, **13**. https://10.3389/fmicb.2022.957066
13. S. Kalathil, M. Rahaman, E. Lam, T. L. Augustin, H. F. Greer and E. Reisner, Solar-Driven Methanogenesis through Microbial Ecosystem Engineering on Carbon Nitride, *Angewandte Chemie International Edition*, 2024, **63**, e202409192. https://doi.org/10.1002/anie.202409192